WILEY-VCH

Title

Terahertz Probing Irreversible Phase Transitions Related to Polar Clusters in $Bi_{0.5}Na_{0.5}TiO_3$-based Ferroelectric

Jiyue Wu[1], Wenfeng Sun[2], Nan Meng[1], Hangfeng Zhang[1], Vladimir Koval[3], Yan Zhang[2], Robert Donnan[4], Bin Yang[2,5], Dou Zhang[6*] and Haixue Yan[1*]*

[1]School of Engineering and Materials Science, Queen Mary University of London, Mile End Road, London E1 4NS, UK

[2]Department of Physics, Beijing Key Lab of Metamaterials and Devices, and Key Laboratory of Terahertz Optoelectronics, Ministry of Education, Beijing Advanced Innovation Center for Imaging Technology, Capital Normal University, Beijing 100048, People's Republic of China

[3]Institute of Materials Research, Slovak Academy of Sciences, Watsonova 47, 04001 Kosice, Slovakia

[4]School of Electronic Engineering and Computer Science, Queen Mary University of London, London E1 4NS, UK

[5]Faculty of Science and Engineering, University of Chester, Thornton Science Park, CH2 4NU, UK

[6]State Key Laboratory of Powder Metallurgy, Central South University, Changsha, Hunan 410083, China

Email: b.yang@chester.ac.uk, dzhang@csu.edu.cn, h.x.yan@qmul.ac.uk

Keywords: terahertz, dielectric, relaxor ferroelectrics, polar cluster, phase transition

Abstract

Electric-field-induced phase transitions in $Bi_{0.5}Na_{0.5}TiO_3$ (BNT)-based relaxor ferroelectrics are essential to the controlling of their electrical properties and consequently in revolutionizing their dielectric and piezoelectric applications. However, the fundamental understanding of these transitions is a long-standing challenge due to their complex crystal structures. Given the structural inhomogeneity at the nanoscale or sub-nanoscale in these materials, dielectric response characterization based on terahertz (THz) electromagnetic-probe beam-fields, is intrinsically coordinated to lattice dynamics during DC-biased poling cycles. The complex permittivity reveals the field-induced phase transitions to be irreversible. This profoundly counters the claim of reversibility, the conventional support for which, is based upon the peak that is manifest in each of four quadrants of the current-field curves. The mechanism of this irreversibility is solely attributed to polar clusters in the transformed lattices. These represent an extrinsic factor which is quiescent in the THz spectral domain.

1. Introduction

Terahertz (THz) radiation (100 GHz to 10 THz) is intrinsically able to probe low-energy lattice phonons [1] and other more complex normal (or collective), modes of solid-phase atomic or ionic assemblies [2], making it ideal for elucidating physical insight into fundamental structural and dynamical variations in dielectric materials.[3] Ferroelectric materials, particularly, are comprised of non-centrosymmetric unit cells, each possessing a switchable polarization of their electric dipole moment. Of the class of ferroelectric materials, perovskite-structured BNT-based (BNT, $Bi_{0.5}Na_{0.5}TiO_3$) has attracted worldwide research interest in recent years with the development of lead-free forms[4] which have been deployed in a range of technological applications including; piezoelectric actuators, sensors and dielectric capacitors. Each of these areas of utility is respectively attributed to their large electric field-induced strain[5], high piezoelectric constant and high specific energy. While the study to-date of the crystal structure and phase transitions of BNT has explained much, there still remain some key points that are controversial due to the complexity of Na-O and Bi-O bonds, and the octahedral tilt in the unit cell[6]. Due to these unique structural properties, phase transitions in BNT, and its derivatives, can be induced by applied electric fields of 10s of $kV.cm^{-1}$[7, 8] which, in most cases, are indirectly illustrated using the bipolar current (*I*-*E*), polarization (*P*-*E*) or strain (*S*-*E*) loops versus the applied electric field.[9] It is now well established that such phase transitions can be direct observed using a variety of in-situ methods, such as X-ray diffraction (XRD)[10], neutron diffraction[11] and, transmission electron microscopy (TEM)[5]. However, the local structural changes (below the nanometre scale), including chemical and displacement disorder, is normally too small for diffraction methods to detect. Consequently, dielectric measurement can be employed as a probe to sense electric-field-induced phase transition.[8] In view of the complexity wrapped up in the dispersive polarizability, there is yet no detailed study of phase transition behaviour of BNT from intrinsic, atomic-level, dielectric action; hence the need for dielectrometry at THz energies.

Conventional dielectrometry is typically deployed over a frequency domain spanning from 1 to 100 MHz. This gleans information of both intrinsic (including lattice transformations), and extrinsic sources (including domain walls, grain boundaries and point defects[12]), of complex dielectric response. Extrinsic factors contribute less to net dielectric response at the higher GHz to THz frequencies due to their long relaxation times, thereby allowing the contribution from intrinsic processes to be isolated and characterized. Furthermore, coherent THz spectroscopy affords simultaneously determination of the real (in-phase), and the complex (quadrature-response manifest as energy-loss by heat), polarization-response to the probe electric field. Understanding the partial contributions from microscopic intrinsic and extrinsic dielectric factors will enable an engineered, and therefore accelerated development and optimization of the aforementioned macroscopic advantages of these important materials.

In this work, BNT-based ($Bi_{0.35}Na_{0.335}Li_{0.015}Sr_{0.3}TiO_3$) ceramics are biased by a DC electric field while being simultaneously probed with a coherent THz beam-field. A new experimental methodology is therefore introduced for the study of phase transitions in ferroelectrics to reveal their intrinsic dielectric response. For the first time, the difference in the THz dielectric behavior of BNT-derived ferroelectrics, before and after the application of a DC electric field, has been observed using THz-Time domain spectroscopy (THz-TDS). THz-TDS revealed that the applied DC electric-field-induced change in the phase transitions of BNT-based ceramics is irreversible and can be ascribed to the crystal chemistry at the sub-nanometer scale.

2. Results and Discussion

The ferroelectric properties of $Bi_{0.35}Na_{0.335}Li_{0.015}Sr_{0.3}TiO_3$ (BNLST) were characterized at different maximum amplitudes of an external DC electric field in order to determine its polarization state and switching dynamics. Relaxor-like slim *P-E* loops with a large field-induced polarization and a negligible remnant polarization are observed (**Figure 1(a)**;

additionally, four current peaks can be observed in the *I-E* curves (**Figure 1(b)**, which show that the largest volume of polar switching and phase transitions takes place inside of the material. Such behaviour is different from that of other classic relaxors and resembles more the features of antiferroelectrics (AFE).[13] From the literature, it appears that the original state of BNLST is more like a non-polar or weak-polar arrangement of electric dipoles.[8] There is no evidence for an AFE ordering in the BNLST ceramics, such as reported in other BNT systems.[14] In addition, the electric-field-induced strain dependence (**Figure 1(c)**) indicates an electrostrictive-like behaviour (linearity of the strain (*S*) *vs*. square of the polarization (P^2) dependence [15]), which is macroscopically coincident with the nonpolar symmetry. In this case, the strain, related to the field-induced transitions, cannot be determined from the measured *S-E* loops. The existence of the four current-peaks in the *I-E* curves can be explained using field-induced phase transition theory:[8] the weak-polar state is transformed to the polar state at certain applied strengths of DC electric field (the peaks in the first and third quadrants), and then this polar state will relax to its original state upon removal of the coercive field (the peaks in the second and fourth quadrants). For this condition, it is generally accepted that the phase transitions in relaxors are reversible and the relaxor is in the 'ergodic' state. However, to-date, there are no studies reporting whether the polar state goes 'completely' or 'partially' back to a weak-polar state after the applied electric field is switched off. The enclosed area of the ferroelectric hysteresis loops cannot be directly linked with the irreversibility of the phase transitions, but it can be related to the loss from friction due to the dipole rotations.

Figure 2 shows the temperature-dependent dielectric permittivity and loss tangent of BNLST at six different frequencies (1, 10, 50, 100 and 500 kHz; and 1 MHz), as measured before and after poling. For the unpoled sample, the anomaly corresponding to the highest permittivity value (denoted as T_m), becomes more pronounced at lower frequencies and shifts to a higher temperature with increasing frequency (**Figure 2(a)**). The strong dispersion of the permittivity

peak is generally accepted as a fingerprint of relaxor behaviour, dominated by relaxation processes of the polar nano-regions (PNRs).[16] PNRs are nanometre-sized regions having a local polarization and existing in the vicinity of T_m.[17] In order to investigate the effect of an external field on PNRs, dielectric measurements were carried out on the same sample after poling in a DC field at 6 kV/mm for 15 minutes, as shown in **Figure 2(b)**. By comparing the dielectric spectra in **Figure 2(a)** and **(b)**, it showed that the ferroelectric relaxor underwent an irreversible transition upon the application of the external electric field. Below T_m, there is a significant increase in the values of the real part of the dielectric permittivity (ε') and loss tangent ($\tan\delta = \varepsilon''/\varepsilon'$) of the poled sample due to the contribution of PNRs to the overall electrical response. It should be noted that the behaviour of PNRs, as discussed here and following, is related to the arrangement of PNRs above the static freezing temperature (T_f). Below T_f, the long-range polar order of these nano-regions is locked after poling. Here, the T_f of PNRs in BNLST is below room temperature, as determined by the dielectric data fitted according to the Vogel-Fulcher law[18]. In addition, the dielectric dispersion completely vanished above T_m after poling. Compared with $\tan\delta$ before poling, the value of $\tan\delta$ decreases sharply at high temperatures (especially above 300 ºC) after poling. The decrease of $\tan\delta$ can be a result of a permanent structure-change after the application of the bias DC electric field. As reported for pure BNT, the monoclinic (*Cc*) phase is suppressed after poling, which enables the rhombohedral (*R*3*c*) structure to be revealed on a global length scale.[19] Meanwhile, the dispersion of $\tan\delta$ diminishes at high temperatures (over 300 ºC) after poling, which is another evidence for the regulation of crystal structure with the help of an external DC electric field. However, no macroscopic phase transitions of BNLST can be directly detected from the dielectric spectrum. T_m cannot be assigned as the critical phase transition point based on the XRD results of BNLST (as shown in **Figure S1**). On a detailed inspection, there is no change in cubic structure (space group *Pm*-3*m*), at room temperature.

Despite the difference in dielectric spectra before and after poling, it is still not possible to definitively claim that the field-induced phase transitions are irreversible at the lattice scale, mainly due to the multiple extrinsic contributions to dielectric behaviour at sub-GHz frequencies. Since intrinsic, lattice-level processes are at the energetics of THz electromagnetic radiation, the phenomenon of reversible or irreversible field-induced phase transitions can be assessed using coherent THz spectroscopy. The BNLST sample has high permittivity and high dielectric losses in the THz spectral band, therefore, two tailored measurement methodologies were implemented: a reflection-based THz measurement configuration and conplane DC biasing. The schematically plot of the reflected THz-TDS set up is presented in **Figure 3** and the technical details are presented in the Experimental Section. A polished, plane-parallel wafer, with a diameter of 13 mm and a thickness of 500 μm, was measured by the THz-TDS systems. As shown in the inset of **Figure 3**, silver paste was applied on opposite edges of a given sample's same surface and served as electrodes, leaving the middle-area of the sample with a 5 mm-wide gap upon which the THz beam-field-spot could fall. The electrodes were connected to a high voltage DC power supply and the poling was taking effect across the middle of the sample surface, where is the effective area THz beam can probe due to the limited penetration depth. Prior to the THz-TDS measurement, the DC electric field was applied for two minutes. The THz beam-field was propagated at normal incidence up to the sample-face (the sample-face being supported parallel to the plane of the optical table). This configuration was adopted to ensure simple kinematic reference of the sample-reflection with respect to the reference-mirror reflection (each resting under its own weight over a supporting rim); i.e. a common optical path length was imposed ensuring that post-processing derivation of complex permittivity was not compromised by phase (path) error, to which THz-TDS is sensitive to. The difference between the sample's reflected signal before and after poling is used to derive the change in dielectric parameters, including permittivity and loss tangent, where the first

differential of permittivity with respect to reflectance was implemented with respect to the following equation[20]:

$$\varepsilon(\omega) = \varepsilon'(\omega) + i\varepsilon''(\omega) = \left(\frac{1+\sqrt{R}}{1-\sqrt{R}}\right)^2:$$

the reflectance, *R*, carries both amplitude and phase information and it is the ratio between the measured sample spectrum and the reference mirror spectrum; ω is angular frequency, $\varepsilon'$and ε'' are the real and imaginary parts of the permittivity, respectively. The detailed procedure of extracting the changes of dielectric parameters is presented in the supplementary information (**Figure S2**).

The real and imaginary parts of the dielectric permittivity of BNLST, as obtained by THz-TDS at 0.4 THz, are shown in **Figure 4**. The voltage was applied in the following cycle: (0, 0.2, 0, - 0.2, 0…1, 0, - 1, 0) kV. This cycle reproduces that of the electric field loading used in ferroelectric hysteresis tests. Herein, it should be noted that the coplane DC bias is unable to create homogeneous electric field distribution on the surface of 5 mm gap area, so the values of electric field are replaced by the real applied DC voltage in the following discussion. There is no change in the dielectric permittivity under ± 0.8 kV, because the applied voltage is too low. When the voltage reached 1 kV, there is a distinct increase in both the real and imaginary parts of the relative dielectric permittivity. This can be explained by the field-induced transitions which take place at 1 kV, resulting in the enhanced ε′ and ε″ due to the intrinsically induced polarization. When the voltage returns to zero, ε′ and ε″ increase again because the dipoles are no longer locked by the bias field (freezing effect) and respond easily to the AC THz beam-field.[21] After the application of the - 1 kV voltage, the values of both ε′ and ε″ are slightly increased, when compared with those after poling at 1 kV. It is worth noting that ε′ further increases after the removal of the applied DC bias field. This is direct evidence that the original polar state of BNLST was changed after the half-cycle of the applied voltage. In other

words, the so-called ‘reversible’ field-induced phase transition is not ‘completely’ reversible. In addition, the drop of ε″ implies that less heat was dissipated due to the reduced friction among the external field-aligned dipoles.

Generally, there are four types of polarization process contributing to the overall dielectric response. They can be sub-divided into two main categories: (i) resonance processes, and (ii) relaxation processes.[22] For resonance, electronic and atomic (ionic) polarizations are involved, whereas the dipolar (orientation) and interfacial (space charge) polarizations contribute to the relaxation.[23] Considering the resonance regime, electronic and atomic polarizations, respectively, result from the oscillatory displacement of the electron cloud and atoms (ions) in response to the probe AC THz beam-field. Thus, both polarization mechanisms can exist at very high frequencies into the infrared (~10 THz) and optical (~1000 THz) spectral domains. On the other hand, the dipolar polarization is related to the rotation of the permanent dipoles under an external AC field and takes place below ~1 GHz.[24] Similarly, the interfacial polarization involves the movement of limited free charge carriers at interfaces or grain boundaries, which respond to low frequency fields (~10s kHz).[22] Therefore, only the electronic and atomic polarization processes contribute to the dielectric response during THz spectroscopy, making it possible to investigate structural changes at the lattice scale. It has been demonstrated that atomic fluctuations contribute to the dielectric response of the THz spectral domain in dielectric systems.[25] The fluctuating atoms in PNRs can be treated as clusters of soft phonons,[26] the so-called polar clusters. The lattice-scale transformation in local polar clusters is suggested as the mechanism for the different THz dielectric response of BNLST ceramics before and after poling. The field-induced evolution of polar clusters inside PNRs is presented schematically in **Figure 4**. Before the poling process (position O), the whole system consists of the PNRs with random orientations of polarization in the non-polar regions. Each PNR is composed of polar clusters with different orientation of polarization at the lattice scale. In BNT-

based materials, it is known that polar clusters originate from the localized in-phase octahedral tilt in the matrix phase.[27] They manifest the existence of the intrinsic lattice instabilities occurring in the ferroelectric due to the random occupancies of the Na^+ and Bi^{3+} ions and the severe difference in the bonding characteristics of Na-O and Bi-O.[28] Hence, it is reasonable to assume that the neighbouring polar clusters do not share exactly the same orientation of polarization due to the lack of long coherence length. This assumption is in an agreement with the recent TEM studies on BNT.[29] Upon poling (**Figure 4**, position A), polarization of the polar clusters is re-aligned along the direction of the applied DC electric field. This means that the lattice instabilities can be theoretically removed under the electric field. It has been reported that the electric field helps to modify the crystal structure in terms of forcing all the ions to irreversibly take up positions compatible with the matrix phase.[19] Moreover, an increased number of activated polar clusters may emerge, which contributes to the enhanced ε'. After the poling process (position B), the polarization of most polar clusters flips back to the original orientation. However, a portion of polar clusters can be inhibited and their polarization deviates from that of the original position. These hindered clusters are believed to be responsible for the irreversible field-induced phase transitions, which intrinsically occur at the lattice scale. Unfortunately, the subtle changes at the PNR level cannot be detected by the THz-TDS because the whole PNR is unable to cohere with a THz field cycle.[30] In addition, the freezing effect from the bias DC electric field is suppressed at room and elevated temperatures, thus the dipoles can respond more freely to the probing AC field and contribute to further increasing of ε'. In addition, after another cycle of poling with a negative DC electric field, more polar clusters become hindered and lattice distortion is further 'tuned', leading to an enhancement of the real part of the permittivity. (Position C).

Summing up the results from the THz-TDS measurements, in the THz spectral domain, there is a detectable change in the dielectric behaviour of BNLST ceramics before and after poling

(**Figure 5**). The difference in the dielectric response can be directly linked with the intrinsic transformation of polar clusters at the atomic level. It was demonstrated that the BNT-based system undergoes field-induced phase transitions which are irreversible after the removal of the applied field. The origin of the field-induced phase transitions is thought to be intrinsic (at the lattice level), coming from polar clusters within PNRs. Considering the correlation length limit of diffraction methods, THz-TDS spectroscopy is demonstrated to be a powerful probe for evaluation of phase transitions in ferroelectrics.

3. Conclusion

The irreversible, bias DC electric-field-induced phase transitions were investigated in BNT-derived ceramics using THz-Time Domain Spectroscopy. In contrast to THz dielectric spectroscopy, the conventional ferroelectric measurements of the *P-E* (*I-E*) hysteresis loops indicated, unconvincingly, that the phase transitions induced by an external electric field are reversible. The differences in the THz dielectric properties of the unpoled and poled samples as well as of the samples subjected to the reverse-poling electric field, suggest the existence of a permanent field-induced lattice transformation, i.e. local polar clusters. It is suggested that these polar clusters within the PNRs are responsible for the observed changes in the THz dielectric spectra. This work is essential in further understanding the intrinsic mechanisms underlying the phase transition behaviour of the BNT-based materials. It provides an innovative approach of applying THz electromagnetic radiation to investigate the phase transition behaviour in ferroelectric systems on the lattice scale.

4. Experimental Section

Sample synthesis: The ceramic samples were prepared via the conventional solid-state method according to the chemical formula, $Bi_{0.35}Na_{0.335}Li_{0.015}Sr_{0.3}TiO_3$ (abbreviated as BNLST). A stoichiometric batch of Bi_2O_3 (99.9% Sigma-Aldrich), Na_2CO_3 (99.5% Sigma-Aldrich), Li_2CO_3

(99.0% Alfa Aesar), $SrCO_3$ (99.5% Alfa Aesar), and TiO_2 (99.8% Sigma-Aldrich) powders were weighed after drying at 200 °C overnight. The ingredients were ball-milled for 4 hours. Calcination of the mixture was carried out in two steps: at 800 °C for 2 hours followed by 900 °C for 4 hours. The calcined powders were ball-milled for another 4 hours and then uniaxially cold-pressed into pellets at 70 MPa. These green discs were finally sintered at 1150 °C for 3 hours. The density of all pellets was measured by the Archimedes method and it reached values above 95% theoretical density.

Electrical Characterization: Electrical measurements were performed on the pellets with silver paste fired on both major sides. The temperature dependence of the real part (ε′) and imaginary part (ε″) of the dielectric permittivity was tested from room temperature up to 500 °C using an LCR meter (Agilent, 4284A, Hyogo, Japan) attached to a PC-controlled furnace. The current-electric field (*I*-*E*), polarization-electric field (*P*-*E*) and strain-electric field (*S*-*E*) loops were measured using a ferroelectric tester (NPL, Teddington, U.K.), at a frequency of 1 Hz and at room temperature.

Reflection based THz-TDS set-up: A femtosecond Ti: sapphire amplifier system with a repetition rate of 1 kHz and a central wavelength of 800 nm was used as a light source. The optical beam was split into a pump beam and a probe beam by a polarizing beam splitter. The pump pulses passing through a chopper were used to generate THz radiation by a conventional electric-optic crystal of ZnTe. The THz beam was focused by a parabolic mirror, and normally applied onto the broad face of the sample. Reflected THz pulses were then collected and steered by the parabolic mirrors and focused onto a ZnTe crystal. The probe optical pulses passed through the same ZnTe detector crystal, a 1/4 wave plate, and a Wollaston prism, respectively. The elliptic polarization emerging from the 1/4 wave late is analyzed by the prism into orthogonal component polarizations of electric vector that are angularly resolved and directed

onto two balanced photodiodes, from which the magnitude and phase of the THz field is deduced.

Supporting Information
Supporting Information is available from the Wiley Online Library or from the author.

Acknowledgments

The authors would like thank the financial support of EPSRC (MASSIVE Project, EP/L017695/1; Teranet EP/M00306X/1), the Grant Agency of the Slovak Academy of Sciences (Grant No. 2/0059/17), China Scholarship Council (CSC, 201506630005) and National Natural Science Foundation of China (51672311, supported by the State Key Laboratory of Powder Metallurgy, Central South University, Changsha, China).

Competing interests
The authors declare no competing financial interests.

Received: ((will be filled in by the editorial staff))
Revised: ((will be filled in by the editorial staff))
Published online: ((will be filled in by the editorial staff))

References

[1] D. Giovanni, W. K. Chong, Y. Y. F. Liu, H. A. Dewi, T. Yin, Y. Lekina, Z. X. Shen, N. Mathews, C. K. Gan, T. C. Sum, *Adv. Sci.* **2018**, *5*, 1800664.
[2] K. V. Tian, B. Yang, Y. Yue, D. T. Bowron, J. Mayers, R. S. Donnan, C. Dobó-Nagy, J. W. Nicholson, D.-C. Fang, A. L. Greer, G. A. Chass, G. N. Greaves, *Nat. Commun*. **2015**, *6*, 8631.
[3] D. S. Rana, I. Kawayama, K. Mavani, K. Takahashi, H. Murakami, M. Tonouchi, *Adv. Mater.* **2009**, *21*, 2881; L. Li, P. Li, N. Lu, J. Dai, X. C. Zeng, *Adv. Sci.* **2015**, *2*, 1500290.
[4] C. Ma, H. Guo, S. P. Beckman, X. Tan, *Phys. Rev. Lett.* **2012**, *109*, 107602; X. Ren, N. Meng, H. Yan, E. Bilotti, M. J. Reece, *Polymer* **2019**, *168*, 246.
[5] X. Liu, X. Tan, *Adv. Mater.* **2016**, *28*, 574.
[6] K. Reichmann, A. Feteira, M. Li, *Materials* **2015**, *8*, 5469.
[7] G. Viola, R. McKinnon, V. Koval, A. Adomkevicius, S. Dunn, H. Yan, *J. Phys. Chem. C* **2014**, *118*, 8564; A. Mahajan, H. Zhang, J. Wu, E. V. Ramana, M. J. Reece, H. Yan, *J. Phys. Chem. C* **2017**, *121*, 5709.
[8] J. Wu, A. Mahajan, L. Riekehr, H. Zhang, B. Yang, N. Meng, Z. Zhang, H. Yan, *Nano Energy* **2018**, *50*, 723.
[9] H. Yan, F. Inam, G. Viola, H. Ning, H. Zhang, Q. Jiang, T. Zeng, Z. Gao, M. J. Reece, *J. Adv. Dielectri.* **2011**, *01*, 107.
[10] J. E. Daniels, W. Jo, J. Rödel, J. L. Jones, *Appl. Phys. Lett.* **2009**, *95*, 032904.
[11] Y. Liu, L. Norén, A. J. Studer, R. L. Withers, Y. Guo, Y. Li, H. Yang, J. Wang, *J. Solid State Chem.* **2012**, *187*, 309.
[12] J. Rödel, W. Jo, K. T. Seifert, E. M. Anton, T. Granzow, D. Damjanovic, *J. Am. Ceram. Soc*. **2009**, *92*, 1153; F. Yang, M. Li, L. Li, P. Wu, E. Pradal-Velázquez, D. C. Sinclair, *J. Mater. Chem. A* **2018**, *6*, 5243.
[13] S.-E. Park, M.-J. Pan, K. Markowski, S. Yoshikawa, L. E. Cross, *J. Appl. Phys.* **1997**, *82*, 1798.
[14] W. Jo, T. Granzow, E. Aulbach, J. Rödel, D. Damjanovic, *J. Appl. Phys.* **2009**, *105*, 094102.
[15] G. Viola, T. Saunders, X. Wei, K. B. Chong, H. Luo, M. J. Reece, H. Yan, *J. Adv. Dielectri.* **2013**, *03*, 1350007.
[16] L. E. Cross, *Ferroelectrics* **1987**, *76*, 241.
[17] G. Xu, Z. Zhong, Y. Bing, Z. G. Ye, G. Shirane, *Nat. Mater.* **2006**, *5*, 134.
[18] H. Vogel, Phys. Z 1921, 22, 645; G. S. Fulcher, *J. Am. Ceram. Soc.* 1925, *8*, 339.
[19] B. N. Rao, R. Datta, S. S. Chandrashekaran, D. K. Mishra, V. Sathe, A. Senyshyn, R. Ranjan, *Phys. Rev. B* **2013**, *88*, 224103.
[20] B. Yang, R. J. Wylde, D. H. Martin, P. Goy, R. S. Donnan, S. Caroopen, *IEEE Trans. Microwave Theory Tech.* **2010**, *58*, 3587; C.-H. Lee, N. D. Orloff, T. Birol, Y. Zhu, V. Goian, E. Rocas, R. Haislmaier, E. Vlahos, J. A. Mundy, L. F. Kourkoutis, Y. Nie, M. D. Biegalski, J. Zhang, M. Bernhagen, N. A. Benedek, Y. Kim, J. D. Brock, R. Uecker, X. X. Xi, V. Gopalan, D. Nuzhnyy, S. Kamba, D. A. Muller, I. Takeuchi, J. C. Booth, C. J. Fennie, D. G. Schlom, *Nature.* **2013**, *502*, 532.
[21] Y. Tan, G. Viola, V. Koval, C. Yu, A. Mahajan, J. Zhang, H. Zhang, X. Zhou, N. V. Tarakina, H. Yan, *J. Eur. Ceram. Soc.* **2019**, *39*, 2064; Z. Yan, D. Zhang, X. Zhou, H. Qi, H. Luo, K. Zhou, I. Abrahams, H. Yan, *J. Mater. Chem. A* **2019**, *7*, 10702
[22] L. Zhu, *J. Phys. Chem. Lett.* **2014**, *5*, 3677.
[23] L. Zhu, Q. Wang, *Macromolecules* **2012**, *45*, 2937.
[24] J. Petzelt, *Ferroelectrics* **2008**, *375*, 156.
[25] T. Tsurumi, J. Li, T. Hoshina, H. Kakemoto, M. Nakada, J. Akedo, *Appl. Phys. Lett.* **2007**, *91*, 182905.
[26] J. Li, H. Kakemoto, S. Wada, T. Tsurumi, H. Kawaji, *J. Appl. Phys.* **2006**, *100*, 024106.

[27] V. Dorcet, G. Trolliard, P. Boullay, *Chem. Mater.* **2008**, *20*, 5061.
[28] V. A. Shuvaeva, D. Zekria, A. M. Glazer, Q. Jiang, S. M. Weber, P. Bhattacharya, P. A. Thomas, *Phys. Rev. B* **2005**, *71*, 174114.
[29] I. Levin, I. M. Reaney, *Adv. Funct. Mater.* **2012**, *22*, 3445.
[30] V. Bovtun, S. Kamba, A. Pashkin, M. Savinov, P. Samoukhina, J. Petzelt, I. P. Bykov, M. D. Glinchuk, *Ferroelectrics* **2004**, *298*, 23.

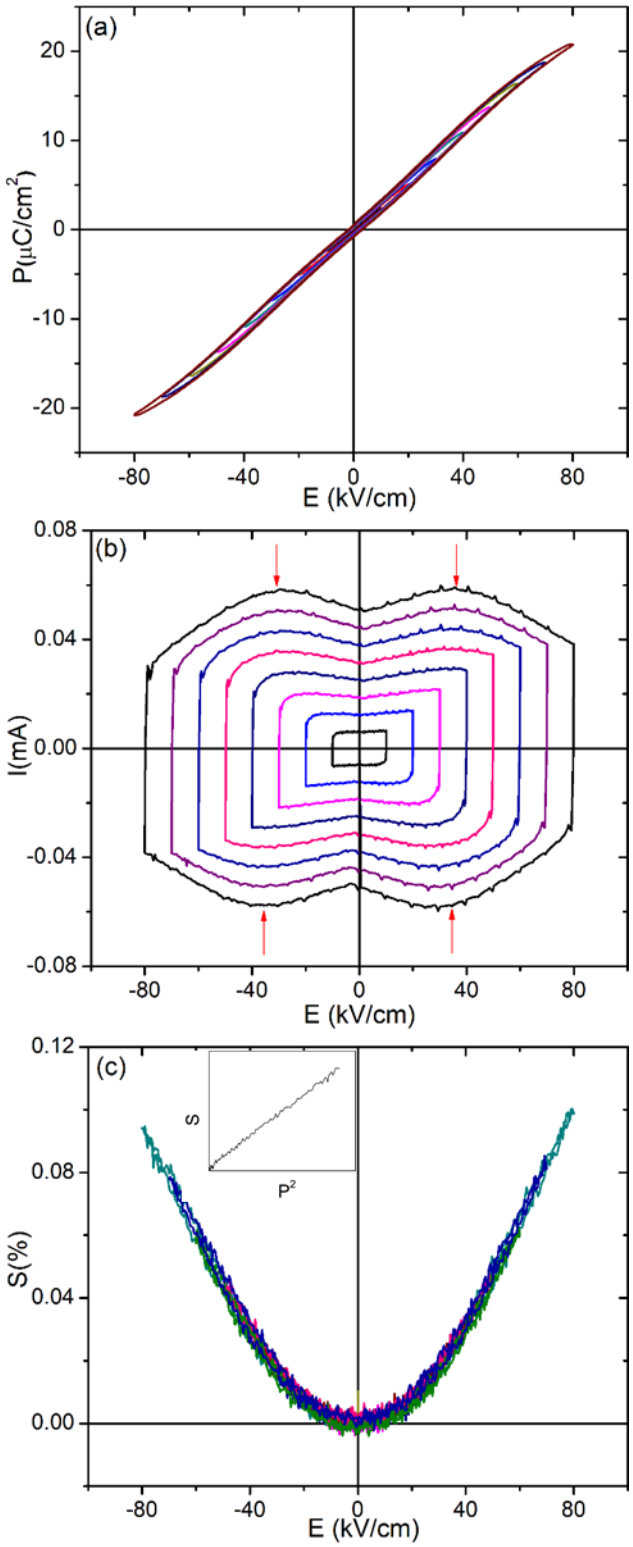

Figure 1 (a) *P*-*E*, (b) *I*-*E* and (c) *S*-*E* loops of BNLST ceramics measured at different electric fields (up to 80 kV/cm) at room temperature and 1 Hz. The insert of (c) shows the linear relationship between the *S* and P^2.

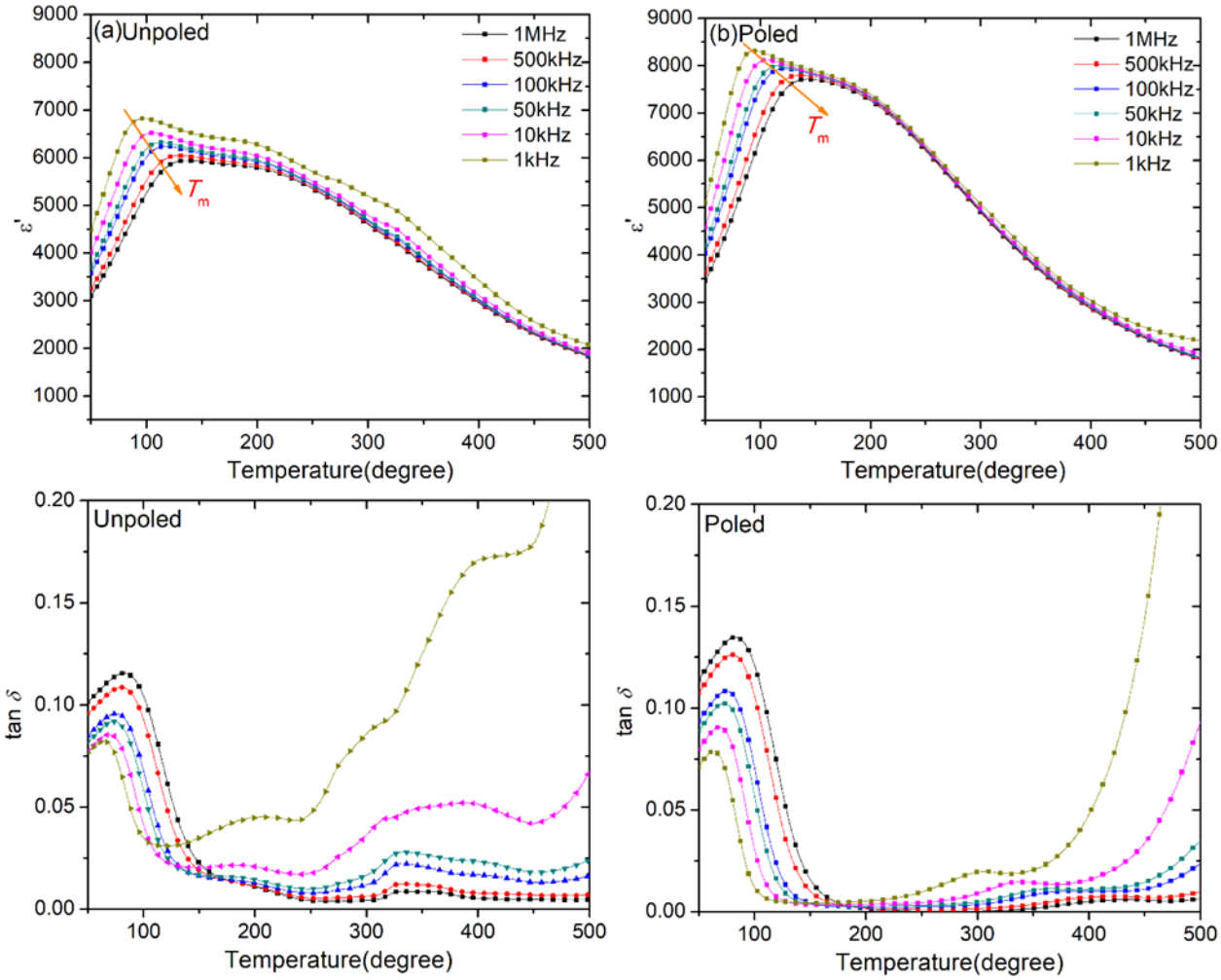

Figure 2 The temperature-dependent dielectric properties of unpoled and poled BNLST ceramics at six different frequencies.

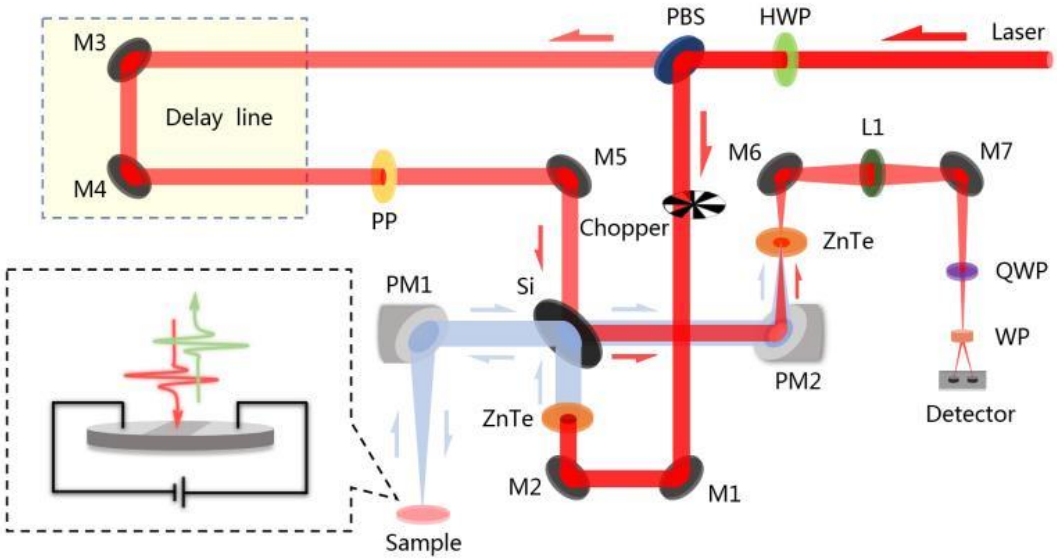

Figure 3 Experimental setup of the reflected THz-TDS spectroscopy: M1~M7, mirrors; PP, polarization plate; PBS, polarization beam splitter; Si, silicon; L1, lens; HWP, half-wave plate; QWP, quarter-wave plate; WP, Wollaston prism; PM1~PM2, parabolic mirrors.

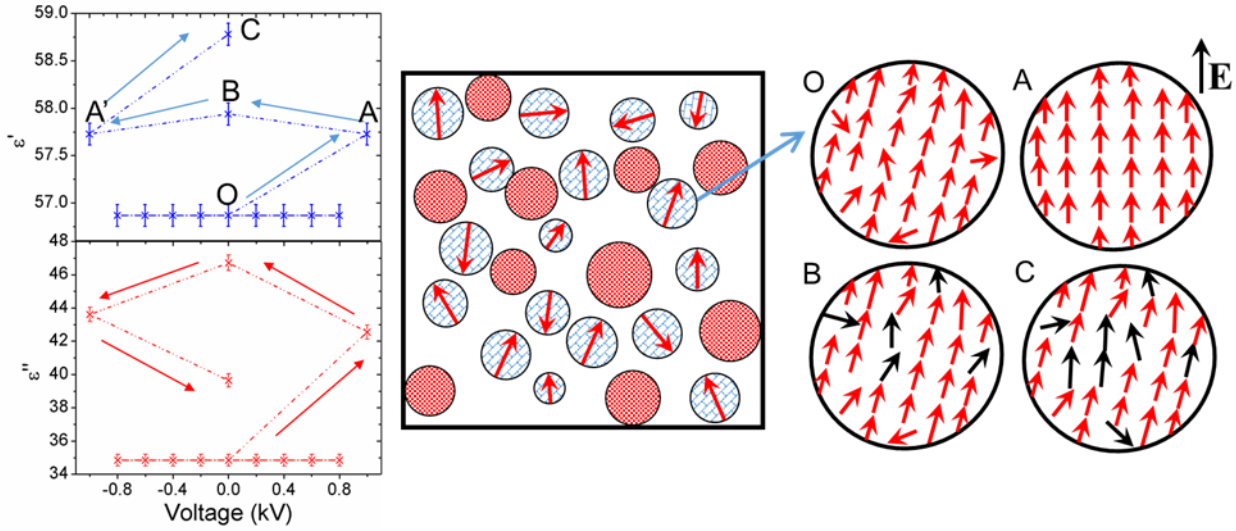

Figure 4 The real part (ε′) and imaginary part (ε″) of dielectric permittivity of BNLST ceramics measured at 0.4 THz with the variation of applied voltage from -1 kV to 1 kV. The sequence of voltage is 0 V, 0.2 kV, 0 V, - 0.2 kV, 0 V, …, 1 kV, 0 V, - 1 kV, 0 V. The schematic drawing illustrates the evolution of the structure at the lattice-level during the whole cycle. The system is considered to be composed of PNRs (circle with an arrow representing the direction of polarization) and non-polar regions (circle with shadow). One representative PNR is magnified before, during and after poling, corresponding to the position O, A, B, C marked in the dielectric diagram, respectively. Each PNR is composed of polar clusters (red arrows representing the direction of spontaneous polarization of each polar cluster and black arrows representing the permanent change of the direction of spontaneous polarization after poling).

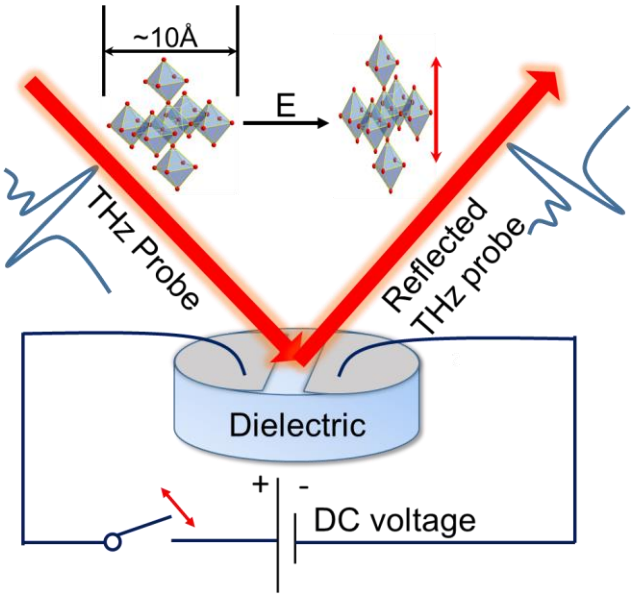

Figure 5 The schematic illustrates the principle of the THz-TDS technique (with the DC bias voltage applied to the target area of the sample). The inset of the figure shows an elongation of a representative oxygen octahedron inside the unit cell of BNLST driven by the field-induced phase transitions.

Table of contents

Terahertz time-domain, reflection-based spectroscopy is implemented to probe the field-induced phase transition dynamics in $Bi_{0.5}Na_{0.5}TiO_3$-based material. The permanent change of the THz dielectric properties detected after the cycle of poling treatment is contributed to from the irreversible sub-nano polar clusters in the transformed lattices, as extrinsic factors and nano-polar regions are unable to respond in the THz region.

Keyword *Materials science*

Jiyue Wu[1], Wenfeng Sun[2], Nan Meng[1], Hangfeng Zhang[1], Vladimir Koval[3], Yan Zhang[2], Robert Donnan[4], Bin Yang[2,5], Dou Zhang[6*] and Haixue Yan[1]*

Title

Terahertz Probing Irreversible Phase Transitions Related to Polar Clusters in $Bi_{0.5}Na_{0.5}TiO_3$-based Ferroelectric

ToC figure

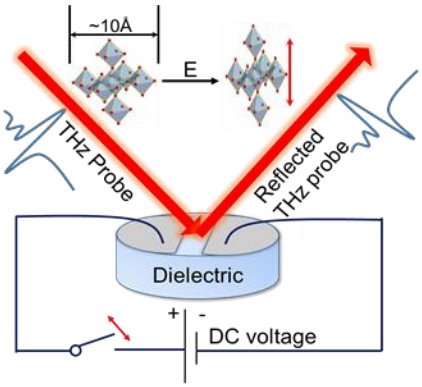

Supporting Information

Title

Terahertz Probing Irreversible Phase Transitions Related to Polar Clusters in $Bi_{0.5}Na_{0.5}TiO_3$-based Ferroelectric

Jiyue Wu[1], Wenfeng Sun[2], Nan Meng[1], Hangfeng Zhang[1], Vladimir Koval[3], Yan Zhang[2], Robert Donnan[4], Bin Yang[2,5], Dou Zhang[6*] and Haixue Yan[1*]*

1. XRD Patterns

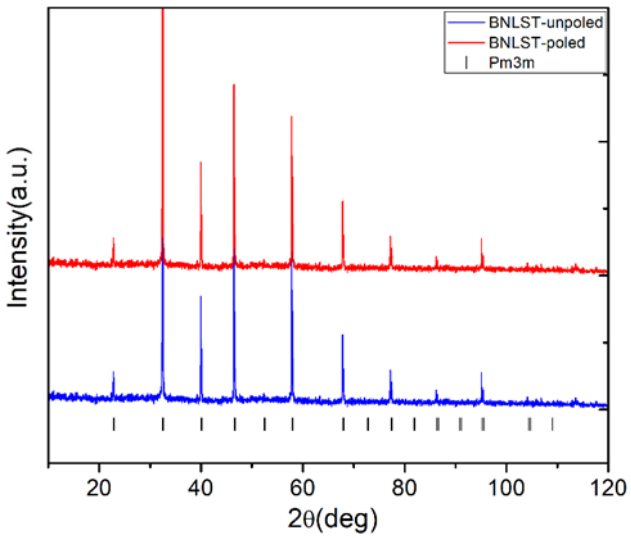

Figure S1 XRD patterns of the unpoled and poled BNLST bulk ceramics measured at room temperature. Both patterns (before and after poling) correspond to the cubic structure (space group *Pm*-3*m*).

2. Reflection Based THz-TDS Test and Analysis

Based on the equation $\varepsilon(\omega) = \varepsilon'(\omega) + i\varepsilon''(\omega) = \left(\frac{1+\sqrt{R}}{1-\sqrt{R}}\right)^2$ [1, 2], differentiation with respect R yeilds:

$$\frac{\Delta\varepsilon(\omega)}{\Delta R} = \frac{R^{\frac{1}{2}}+1}{R^{\frac{1}{2}}} \cdot \left(R^{\frac{1}{2}}-1\right)^2 - \frac{\left(R^{\frac{1}{2}}+1\right)^2}{R^{\frac{1}{2}} \cdot \left(R^{\frac{1}{2}}-1\right)^3}$$

where: R is the measured reflection coefficient of the sample with respect to the reflection reference mirror; ΔR is the difference between $R_{poledsample}$ and $R_{unpoled}$; R, furthermore, is complex vector conveying both amplitude and phase information. The time-domain scan was focused on the peak-pulse only and gave the best system dynamic range at 400 GHz.

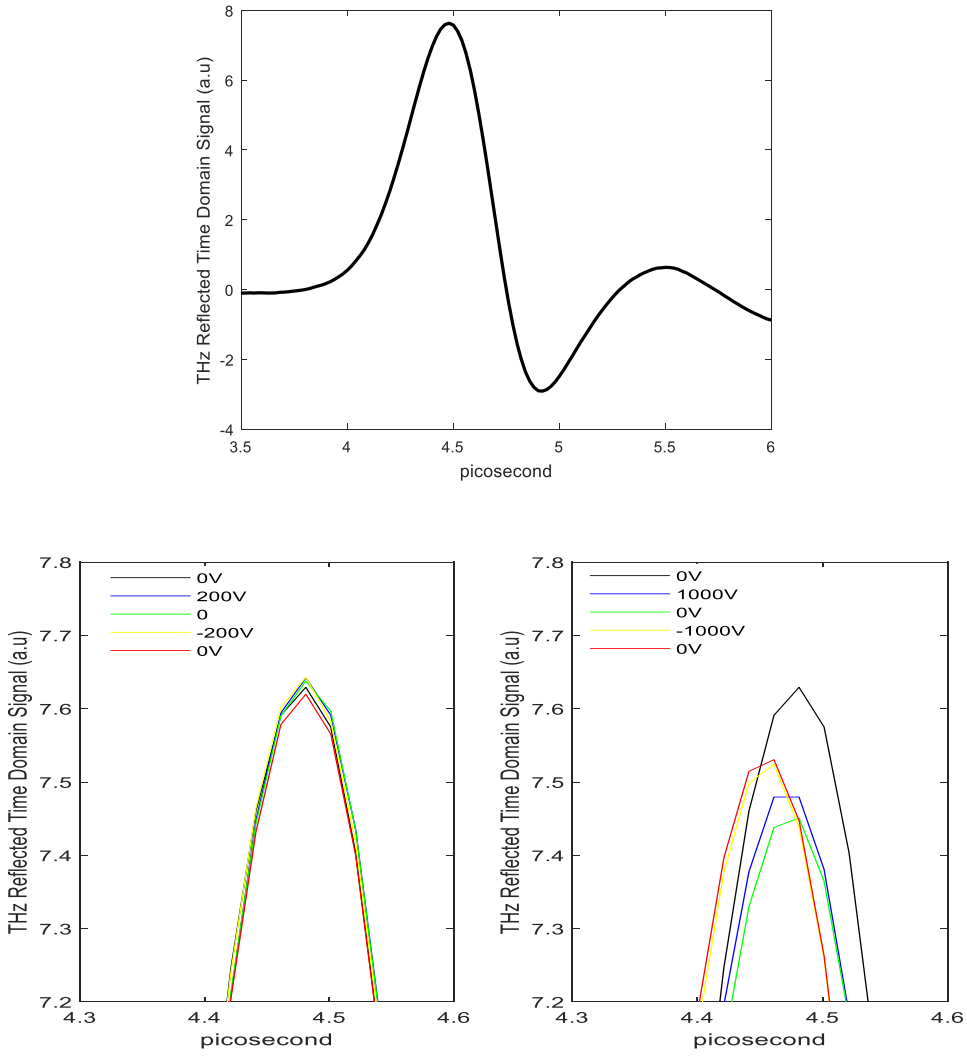

Figure S2 The measured peak (top) of the reflection-based THz Time Domain Pulse after the poling cycle of low electric voltage (left, zoomed in), and high electric voltage (right, zoomed in). The time resolution is 0.02 picoseconds. The black line is the result of the initial unpoled sample.

References:

[1]B.Yang, R.Wylde, D.Martin, P.Goy, R.Donnan and S.Carpooen, *IEEE Trans. Microwave Theory Tech.* **2010**, *58*, 3587

[2] C.-H. Lee, N. D. Orloff, T. Birol, Y. Zhu, V. Goian, E. Rocas, R. Haislmaier, E. Vlahos, J. A. Mundy, L. F. Kourkoutis, Y. Nie, M. D. Biegalski, J. Zhang, M. Bernhagen, N. A. Benedek, Y. Kim, J. D. Brock, R. Uecker, X. X. Xi, V. Gopalan, D. Nuzhnyy, S. Kamba, D. A. Muller, I. Takeuchi, J. C. Booth, C. J. Fennie, D. G. Schlom, *Nature.* **2013**, *502*, 532.